

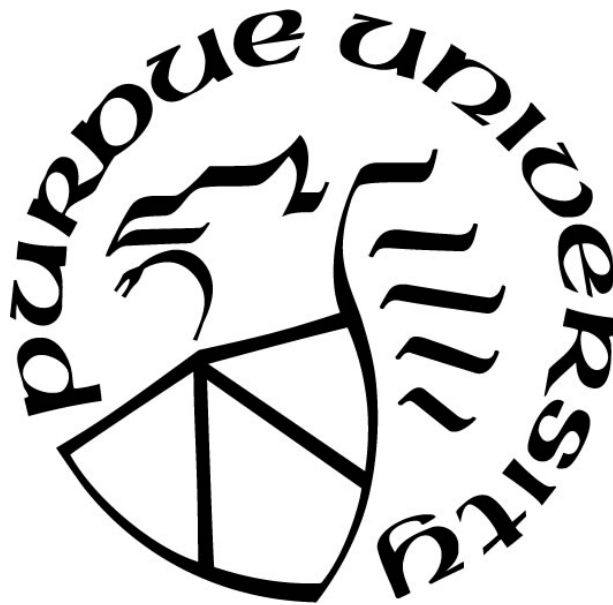
STUDY OF INCLUSION REMOVAL IN A GAS-STIRRED LADLE

by
Wenjie Liu

A Thesis

*Submitted to the Faculty of Purdue University
In Partial Fulfillment of the Requirements for the degree of*

Master of Science in Engineering



Department of Mechanical and Civil Engineering

Hammond, Indiana

December 2018

**THE PURDUE UNIVERSITY GRADUATE SCHOOL
STATEMENT OF COMMITTEE APPROVAL**

Dr. Chenn Q. Zhou, Chair

Department of Mechanical and Civil Engineering

Dr. Harvey Abramowitz

Department of Mechanical and Civil Engineering

Dr. Xiuling Wang

Department of Mechanical and Civil Engineering

Approved by:

Dr. Chenn Q. Zhou

Head of the Graduate Program

TABLE OF CONTENTS

TABLE OF CONTENTS.....	3
LIST OF TABLES.....	5
LIST OF FIGURES	6
LIST OF SYMBOLS	7
ABSTRACT.....	9
CHAPTER 1. INTRODUCTION	11
1.1 Background of inclusion formation	11
1.2 Literature Review.....	12
1.2.1 Literature review on gas-stirred flow inside ladle	12
1.2.2 Literature review on inclusion removal mechanism.....	13
1.3 Objective.....	15
CHAPTER 2. METHODOLOGY AND CFD MODELS.....	17
2.1 Methodology.....	17
2.2 Assumptions of Simulation.....	18
2.3 Multiphase Flow Models	18
2.3.1 CFD model for gas-stirred flow.....	18
2.3.1.1 Continuity equation	19
2.3.1.2 Momentum equation.....	19
2.3.1.3 Turbulence model.....	20
2.3.1.4 Discrete phase model [25]	20
2.3.2 CFD model for inclusion behavior	23
2.3.2.1 Population balance model.....	23
2.4 Multiphase Flow Validation	25
2.4.1 Comparison Results.....	26
CHAPTER 3. GAS-STIRRED LADLE INCLUSION REMOVAL SIMULATION	27
3.1 Computational Domain.....	27
3.2 Boundary Conditions	28
3.3 Results and Analysis of Baseline Case Simulation.....	29
3.3.1 Multiphase Flow development	30

3.3.2	Gas bubble distribution analysis	31
3.3.3	Flow characteristics	32
3.3.4	Inclusion removal analysis	33
3.4	Parametric Study	37
3.4.1	Inclusion size	37
3.4.2	Results comparison	38
3.4.3	Analysis of different removal mechanisms	39
CHAPTER 4. CONCLUSIONS.....		40
4.1	Conclusions.....	40
LIST OF REFERENCES		41
PUBLICATIONS.....		44

LIST OF TABLES

Table 1.1 Summarizing of CFD model of inclusion growth and removal.....	14
Table 2.1 Initial conditions for full-scale ladle.....	26
Table 2.2 Flow model validation	26
Table 3.1 Inclusion removal ratio of different inclusion size	38
Table 3.2 Comparison between Lou et al.'s CFD with current work.....	38

LIST OF FIGURES

Figure 1.1 Steps in Ladle Treatment[1]	11
Figure 2.1 Diagram of the ladle	17
Figure 3.1 Computational domain of Nucor Decatur gas-stirred ladle.....	27
Figure 3.2 Calculation Mesh: a) front view b) bottom view.....	28
Figure 3.3 Multiphase flow a) The volume fraction of three phases b) The velocity of steel	29
Figure 3.4 Slag movement within the first 30s inside the ladle for Baseline Case (Q = 5scfm)..	30
Figure 3.5 Effect of argon gas flow rate on slag eye size	31
Figure 3.6 Gas bubble development: (a) contour of gas bubble diameter. (b) Bubble weight percentage	31
Figure 3.7 Bubble diameter distribution based on weight percentage of total weight of bubbles.	32
Figure 3.8 Flow behavior: Streamline at the center planes.....	33
Figure 3.9 Inclusion concentration distribution with a radius of 5 μ m at 100s, 300s.....	34
Figure 3.10 Overall inclusion number density change with gas blowing time.....	35
Figure 3.11 Effect of different mechanism on inclusion removal efficiency	36
Figure 3.12 Inclusion removal to the wall and slag	36
Figure 3.13 The inclusion number density change of different inclusion size with times	37
Figure 3.14 The inclusion removal efficiency due to various mechanisms for 5 μ m, 10 μ m 50 μ m inclusion size.....	39

LIST OF SYMBOLS

ρ_i	Density (kg/m ³)
α_i	Volume fraction
$\bar{\mathbf{u}}_i$	Averaged velocity vector (m/s)
S_i	Mass source (kg·m ⁻² ·s ⁻¹)
$\bar{\mathbf{M}}_i$	Interaction force
$\bar{\bar{\tau}}_i$	Stress-strain tensor (N/m ²)
μ_i	Viscosity (kg·m ⁻¹ ·s ⁻¹)
\vec{g}	Gravity acceleration
P	Pressure (Pa)
F_D	Drag force (N)
D_b	Bubble diameter (m)
d_b	Bubble diameter (m)
Re	Reynold's number
C_{VM}	Virtual mass factor
k	Turbulent kinetic energy (m ² /s ²)
ε	Dissipation rate of turbulent kinetic energy (m ² /s ²)
G_j	Production of turbulence kinetic energy (m ² /s ²)
C_D	Drag coefficient
Q	Volume flow rate (m ³ /s)
σ	Surface tension (N/m ²)
C_1	Dimensionless constant
τ_{rel}	Relaxation time (s)
τ_k	Turbulent microscale (s)
ν	Kinematic viscosity (kg·m ⁻¹ ·s ⁻¹)
I	Turbulence intensity (%)
τ_B	Breakup time scale (s)
τ_C	Coalescence time scale (s)
$n(V_i)$	Number density of inclusion (n/m ³)
$\beta(V_i, V_j)$	Inclusion coalescence rate
V_i	Inclusion volume (m ³)
S_{eff}^{p-g}	Capture efficiency of turbulent shear collision
C_p	Specific heat capacity (J·g ⁻¹ ·K ⁻¹)
D_{o2}	Diffusivity (m ² ·s ⁻¹)
F	Force (N)
h	Convective heat transfer coefficient (W·m ⁻² ·K ⁻¹)
w	Relative velocity (m·s ⁻¹)
Nu	Nusselt number
R	Bubble radius (m)
Pr	Prandtl number
T	Temperature (K)
t	Contact time (s)

ε_p Particle emissivity
 θ_R Radiation temperature (K)

ABSTRACT

Author: Liu, Wenjie. MSE
Institution: Purdue University
Degree Received: December 2018
Title: Study of Inclusion Removal in a Gas-stirred Ladle
Major Professor: Chenn Q. Zhou

Steel refining via ladle treatment is critical to final product quality in the steel manufacturing process. The process of ladle refining serves to assist in the removal of non-metallic inclusions, which can impact steel product fatigue strength, impact toughness, and corrosion resistance. While the steelmaking industry has in place best practices for the process, it remains costly to performing trial and error testing on the ladle. In addition, an understanding of the flow phenomena within the ladle during operation can provide industry with key knowledge necessary to improve the efficiency and throughput of the process.

The method by which this research aims to address this is through the development of a comprehensive computational fluid dynamics (CFD) model of the steelmaking ladle. Such a model, capable of predicting the inclusion removal process and flow patterns within the ladle, would serve to provide the necessary information to advance steelmaking efficiency and improve product quality. A full scale unsteady state three dimensional CFD model has been developed to predict removal of inclusion during gas-stirring in a ladle. The Eulerian-Eulerian model was used to simulate the multiphase flow, the Population Balanced Model (PBM) has been used to describe the inclusion distribution. The phenomena of bottom-blow argon bubble coalescence and breakup were considered.

Additionally, a model has been developed to predict inclusion removal during operation. For the inclusion removal model, the CFD-PBM coupled method has been proposed to investigate the inclusion behavior. This includes representing phenomena such as inclusion-bubble collision, inclusion removal by attachment to the ladle refractory, and inclusion capture by slag floating on

the surface of the melt. The unified computational model for simulation of fluid flow and inclusion removal was validated against industry measurements provided by Nucor Steel.

Using this CFD model and a ladle geometry and set of baseline conditions provided by Nucor Steel, studies were carried out to examine flow development, gas bubble distribution, and inclusion removal. Examining the impacts of inclusion size on removal rate indicated that larger inclusions are removed faster. This agreed with both industry expectations and data found in published literature. In addition, the model predicts that bubble-inclusion collision are primarily responsible for 99% inclusion removal in a gas-stirred ladle.

CHAPTER 1. INTRODUCTION

Ladle treatment technology develops two main routes after a long process: Electromagnetic Stirring (EMS) Ladle and Gas-stirred Ladle. Top-injected and bottom-injected gas-stirred ladle are two main different types of gas-stirred Ladle. The bottom-stirring ladle has been most widely used. The argon gas bubble from bottom porous plugs generates the recirculation flow pattern enhances turbulent mixing and transport inclusion to top slag/steel interface and support the slag phase to absorb the inclusions.

In the steelmaking process, a huge amount of non-metallic inclusion (most of them are alumina) is generated. In order to produce steels with low total oxygen content, the effective inclusion removal is required during ladle treatment. The most common ladle treatment steps include deoxidation of the steel and slag, alloying the steel, adjusting the steel temperature for shipping to caster, inclusion modification and inclusion removal. The simplified ladle treatment steps are expressed in Figure 1.1.

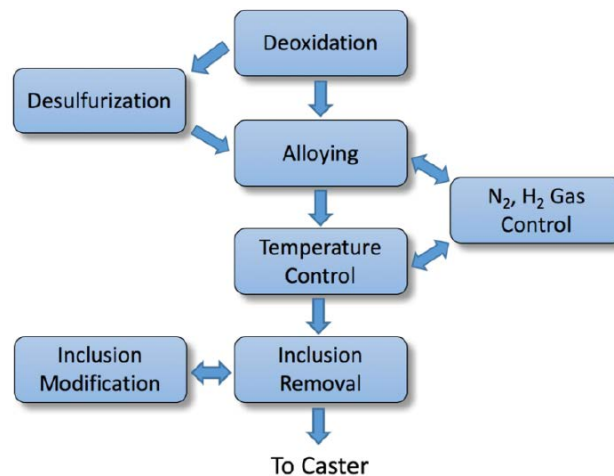
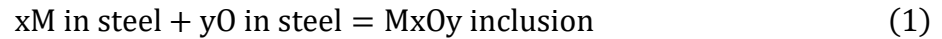


Figure 1.1 Steps in Ladle Treatment[1]

1.1 Background of inclusion formation

In order for steel to be cast continuously, oxygen in the liquid steel must be reduced to avoid CO formation during solidification [1]. The aluminum, as a common element in deoxidation, has been used in this study. The oxygen content of the steel widely varies. Typical oxygen level of BOF

and EAF can range from 200 to 800 ppm [2] . When de-oxidant is added to the steel, the oxygen in the steel reacts with the de-oxidant addition to form an oxide:



Homogeneous nucleation of oxides will occur when the level of dissolved metal and oxygen is high. The nucleation rate is influenced by the interfacial energy of deoxidation product in contact with steel. It is generally accepted that nucleation occurs very quickly and a strong relationship between the oxygen concentration and inclusion size has been found. The early stages of inclusion formation is controlled by oxygen diffusion in the liquid metal [3] .

1.2 Literature Review

The goal of this study is to discuss the complicated inclusion removal phenomena with multiphase flow inside the gas-stirred ladle. There are two categories of numerical research among the inclusion removal mechanism: Inclusion removal by attaching refractory and capturing by top slag, and the study on the including-bubble collision mechanism, the comprehensive argon bubble coalescence and break-up model has been employed to predict bubble behavior.

1.2.1 Literature review on gas-stirred flow inside ladle

Numerous experimental and numerical studies have been conducted for gas-stirred flow in order to understand transient multiphase flow. In addition, greater attention has been directed to bubble behavior description and the effect of argon gas physical characteristics.

Szekely et al. [4] using a simplified water-air model modeled a fluid dynamics gas-stirred ladle. The Spalding's $k-\omega$ turbulence model has been used to describe turbulence flow inside the system. The injected bubbles, which with constant diameter, were focused in a cylindrical region. Then Debroy et al. [5] developed the methodology to model bubble dispersion within a column of constant diameter via connecting the gas volume fraction to the injection rate from the argon plug. Then, Johansen et al.[6] used experiments method studied a cylindrical water model of a ladle with porous plug, which located at the center bottom of the ladle, injecting air. By using this approach, it was witnessed that the flow velocity in the two-phase bubble area is affected by bubble turbulence kinetics. An in-depth review of the mechanisms of energy dissipation phenomena was

presented by Mazumdar et al. [7] It was found that bubble friction and slippage at the ladle wall were influential in energy dissipation, the combination of them contributing around one-third of total energy input; the rest two-third was divided by the turbulence induced through injected gas in melt, and interaction between the slag phase and the steel phase. Zhang et al. [8] developed a full scale three dimensional gas fluid flow model based on the two phases Euler-Euler approach for gas-stirring system. From his study, turbulence was simulated by using standard k- ϵ model, air and water were considered as two different continuous phases. They share space presented by their volume fraction. The effects of different drag force model of turbulent model, the bubble size were compared; and the injection of gas method into the liquid phase has been analyzed. Argon bubble behavior and movement have also elicited interest over the past several years. Cloete [9] used the Eulerian-Lagrangian method to simulate the gas injection behavior, the simulation results of the flow pattern considering heat transfer in the jet flow has been validated with the experimental work. The gas phase is considered as discrete phase like small particles by using the Lagrange approach. Based on the real condition, the small bubble formed during the high velocity gas penetrate process. Cao and Nastac [10] compared in detail the Euler-Euler and Euler-Lagrange approaches on simulating multiphase flow in both water model and full scale ladle system. Through comparing the experimental work measurements and computational simulation results, the Euler-Lagrange model has been demonstrated is more accurate for describing the interface shape. Guo et al. [11] developed a small scale three-dimensional, gas-liquid flow model by using Eulerian- Lagrangian approach in a ladle. In this model, the inclined lift force is included to explain the bubble plume spreading. The inclined drag forces is also extended to include the mass transfer between the floating bubble and free surface.

1.2.2 Literature review on inclusion removal mechanism

In recent decades, a number of models have been developed to describe inclusion growth and removal. As for the inclusion removal mechanism, in general, the inclusion in liquid steel are mainly removed by three mechanism [12] . Since the mid-1970s, computational fluid modeling results from gas-stirred ladles began to be employed for calculating the inclusion removal and growth. Table 1.1 shows the former studies [13] -- [18] on inclusion removal and growth during gas-stirred ladle.

Table 1.1 Summarizing of CFD model of inclusion growth and removal.

Reference	Year	Turbulence model	Heat flow	Dimension	Growth			Removal			Stirring
					Turbulence	Stokes	Shear	Gas bubble	To slag	To refractory	
Nakanishi & Szekely	1975	k- ϵ	No	2D	Yes	No	No	No	No	No	Gas
Shirabe & Szekely	1983	k- ϵ	No	2D	Yes	No	No	No	Yes	No	Gas
Johansen et al	1986	k- ϵ	No	2D	No	No	No	No	Yes	Yes	Gas
Hodgson	1996	k- ϵ	No	3D	Yes	Yes	No	No	No	Yes	Gas
Wakoh et al	1999	k- ϵ	No	3D	Yes	Yes	Yes	Yes	No	No	Gas
Miki & Thomas	1999	k- ϵ	Yes	3D	Yes	Yes	No	Yes	No	No	Gas

Some quite comprehensive CFD models both considering inclusion growth and removal, have been developed in recent years. A 2D two phase model has been developed by Sheng et al.[19] . The inclusion removal from the top slag layer, removal to the refractory lining and removal by bubble flotation have been conducted, and three flotation models have been introduced to describe inclusion floating process. The results showed that bubble-inclusion buoyancy collision is the most common collision method when the inclusion diameter is between 5-50 μm , which is the most common inclusion in ladle. SÖder and JÖnsson [20] enhanced the mechanisms of bubble-inclusion interaction including turbulence random collision, stokes collision and laminar shear collision, turbulence random collision are most commonly applied in colliding of particles in turbulent flow; Stokes turbulence collision happens because of the density difference between liquid steel and inclusion; laminar shear collision is for small (usually smaller than 10 μm) inclusions in different streamlines, because the different path of the slow inclusion may have the chance to catch up the faster inclusion. Lou et al. [21] employed Population Balance Model (PBM) to describe inclusion behavior, with constant bubble injection. Inclusion were divided into several groups according to

their sizes, multiple mechanisms for inclusion-bubble interaction (basically is inclusion-bubble collision) have been considered. Wang et al. [22] determined that the detailed inclusion removal procedure, inclusion can attach to bubble and be carried up to the slag layer. The overall inclusion removal probability through attached with bubble and be carried to the slag-steel surface is predicted by three probabilities:

$$P = P_a * P_c * (1 - P_d) \quad (2)$$

Where P_a , P_c and P_d represent the attachment probability between bubble and inclusion, collision probability and detachment probability, the probability of detachment can be set to zero because the detachment is insignificant.

To sum up, a lot of progress have been made in the study of inclusion-bubble interaction and inclusion-inclusion interaction mechanism. However, due to the complex behavior of the argon bubble, there are few studies combined the bubble coalescence and break-up model with inclusion-bubble interaction mechanism. Because of the large computational time, the full-scale numerical simulation is difficult to conduct. Under reasonable assumptions, the study on the inclusion removal and argon bubble behavior investigation inside the gas-stirred ladle is meaningful.

1.3 Objective

Most of the current numerical simulation work focuses on the theory of inclusion removal mechanisms, the water model simulation has been usually conducted. The full-scale unsteady state gas-stirred ladle simulations are rare. Two parts of the work have been conducted in this study, one is gas-stirred flow and another one is inclusion removal inside ladle.

For the first part, the full-scale flow simulation based on the Nucor Steel gas-stirred ladle is conducted by using Eulerian-Eulerian method. The argon bubble injection and bubble behavior is investigated, the CFD model has been validated by comparing the simulation result with the industry measurements.

For the second part, the flow field calculated for part one has been imported. In order to save calculation time, the flow is frozen during the inclusion removal process. Comprehensive

mechanisms of inclusion removal and detailed inclusion-bubble interaction were conducted. The effect of inclusion size was investigated.

CHAPTER 2. METHODOLOGY AND CFD MODELS

2.1 Methodology

Figure 2.1 shows the structure of Nucor Steel Co., Ltd gas-stirred ladle [23] . The ladle is a cylindrical vessel, two porous plugs are located at the bottom of the ladle in order to inject argon into the steel bath. Three phases including steel, slag and air phase can be witnessed.

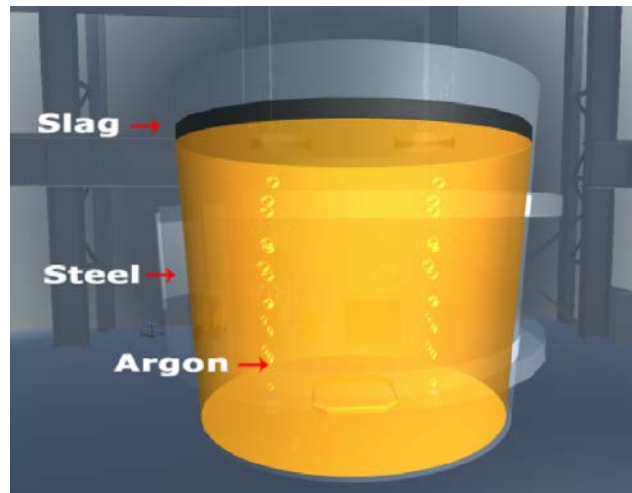


Figure 2.1 Diagram of the ladle

The Eulerian-Eulerian approach coupled with the Population Balanced Model (PBM) is applied. The gas-stirred ladle model including liquid steel, slag, argon bubble, and the atmospheric air. Based on the Eulerian-Eulerian method, the mass conservation equation and momentum conservation equations are used for each phase separately. The Discrete Phase Model (DPM) is employed to track the each argon bubble movements. The turbulence flow is presented by using the realizable $k - \epsilon$ turbulent model. The virtual mass forces, pressure gradient forces, and drag forces are simulated as well. Two-way coupling method has been discussed; the discrete random walk model has been used to predict the bubble movement turbulence effects. PBM, which is acted as the additional source term, has been added into overall inclusion number density transport equations. The PBM has ability to account for the inclusion removal and predict the size distribution of the inclusion.

2.2 Assumptions of Simulation

The numerical model of multiphase flow and inclusion behavior in a gas-stirred system is developed based on the expressing assumptions:

- a) The liquid steel inside the ladle is considered as incompressible Newtonian fluid, and the turbulent flow shows the same characters for all directions.
- b) The effects of top slag chemistry is small and can be ignored, and a pressure outlet has been assumed at the top of ladle.
- c) The inclusion formation rate is dinky and the inclusion generation in ladle through refractory, entrapment of top slag, or nucleation reaction is neglected.
- d) The inclusion-inclusion interaction including formation and growth has been ignored, the constant inclusion size has been assumed.
- e) Inclusion transporting to the slag is considered 100% absorption probability by the slag layer; inclusion reaching slag eye (mean value of two slag diameter area) is assumed revert back into the ladle.
- f) Once the flow reach the quasi steady-state condition, the size and form of slag eye does not change with time during the bubble move to the top surface.

2.3 Multiphase Flow Models

2.3.1 CFD model for gas-stirred flow

During the gentle gas-stirring process, a series of complicated multiphase flow phenomena will occur inside the ladle, including argon bubbles coalescence and break-up. The choice of suitable numerical models to present those phenomena is significant to this study of the inclusion removal process.

The multiphase Eulerian-Eulerian model was introduced in this study in order to couple with PBM. This method overcome the limitation of the VOF model because the VOF method sharing the mountain equation for all phases, and also allows the usage of discretization theories and options suited to both sharp and dispersed interface regimes.

2.3.1.1 Continuity equation

Based on the Eulerian–Eulerian approach, the conservation of mass and conservation of momentum are applied for each phase. Among these three phases, the interaction forces in a gas-stirred system are treated as momentum exchange source terms.

$$\frac{\partial}{\partial t} (\alpha_i \rho_i \vec{u}_i) + \nabla \cdot (\alpha_i \rho_i \vec{u}_i) = S_i \quad (3)$$

where α_i , ρ_i , \vec{u}_i , and S_i are the volume fraction, density, velocity vector, and mass source term of molten steel ($i = m$), slag ($i = s$), gas ($i = g$), and inclusion particle ($i = p$), respectively. S_m , S_s and S_g are zero, because the mass of those no longer change with time and S_p is calculated from PBM of inclusion and calculated subsequently. The volume fraction α_i , represent the space token by each phase. The description of the multiphase flow as an interpenetrating continuum incorporates the concept of phase volume fraction.

$$\sum_{i=0}^n \alpha = 1 \quad (4)$$

2.3.1.2 Momentum equation

The interaction forces among three phases in a gas-stirring system are considered as momentum exchange source terms in the momentum equations. The momentum equation for phase i yields:

$$\frac{\partial}{\partial t} (\alpha_i \rho_i \vec{u}_i) + \nabla \cdot (\alpha_i \rho_i \vec{u}_i \vec{u}_i) = -\alpha_i \nabla p + \nabla \cdot \bar{\tau}_i + \alpha_i \rho_i \vec{g} + \vec{M}_i \quad (5)$$

Where $\bar{\tau}_i$ is the stress-strain tensor of the i th phase:

$$\bar{\tau}_i = \alpha_i \mu_{eff} (\nabla \vec{u}_i + \nabla \vec{u}_i^T) \quad (6)$$

$$\mu_{eff} = \mu_i + C_{\rho i} \frac{k^2}{\varepsilon} \quad (7)$$

Here, μ_i and μ_{eff} are the viscosity of phase i , \vec{g} is the gravity acceleration; p is the local pressure, which is shared by all three phases; and \vec{M}_i is interaction force existing at the three phases

The drag force, F_D , is written as:

$$F_D = \frac{18\mu C_D Re}{\rho_p d_p^2} \frac{1}{24} \quad (8)$$

Where d_p the bubble size presented by diameter, Re is the relative Reynolds number. The additional acceleration terms, which including the virtual mass force, can be expressed as follow:

$$\vec{F}_{VM} = -C_{VM} \frac{\rho}{\rho_p} \left(\vec{u}_p \nabla \vec{u} - \frac{d\vec{u}_p}{dt} \right) \quad (9)$$

where C_{VM} a constant value 0.5 presenting the virtual mass factor.

2.3.1.3 Turbulence model

There is a turbulent flow inside the three phases. Because of that, the choice of appropriate turbulence model to simulate the multiphase flow is critical to this study of the gas-stirred process. Yan [24] employed different models to simulate the turbulence flow in bottom-blowing bubble condition and compared different turbulence model with the water model experiment measurements. The results shows the Realizable k- ε turbulence model has the outstanding performance on predicting the bottom blowing gas-stirring system.

$$\frac{\partial \rho k}{\partial t} + \frac{\partial \rho \mu_j k}{\partial x_j} = \frac{\partial}{\partial x_j} \left(\frac{\mu_T}{\sigma_k} \right) \frac{\partial k}{\partial x_j} + G_j - \rho \varepsilon \quad (10)$$

$$\frac{\partial \rho \varepsilon}{\partial t} + \frac{\partial \rho u_j \varepsilon}{\partial x_j} = \frac{\partial}{\partial x_j} \left(\frac{\mu_T}{\sigma_\varepsilon} \right) \frac{\partial \varepsilon}{\partial x_j} + \frac{\varepsilon}{k} (C_{\varepsilon 1} G_j - G_{\varepsilon 2} \rho \varepsilon) \quad (11)$$

where k is the turbulent kinetic energy and ε is the dissipation rate, both for the liquid phase; G_j contributes turbulence kinetic energy production because of the liquid phase induced shearing.

2.3.1.4 Discrete phase model [25]

The DPM model is used for the trajectory of every individual particle by integrating the force balance. By using two-way coupling method, the potential buoyance energy included at the argon bubble can be moved around to the continuous phases as a additional source term. For tracking the bubble, each bubble is calculated by satisfying the force balance equation, written in a Lagrangian reference frame, expressed as following equation:

$$\frac{d\vec{u}_p}{dt} = F_D (\vec{u} - \vec{u}_p) + \frac{\vec{g}(\rho_p - \rho)}{\rho_p} + \vec{F}_{VM} + \frac{\rho}{\rho_p} (\vec{u}_p \nabla \vec{u}) \quad (12)$$

Where the ρ_p is the argon gas density for particle. The terms on the equation right side express drag force, buoyancy, virtual mass, and pressure gradient force. Bottom injected bubble contributes to momentum enchantment between different continuous phases by bubble motion

force and can be added as a source term (F_b) in the momentum conservation equation. The drag force, F_D , is written as:

$$F_D = \frac{18\mu C_D Re}{\rho_p d_p^2} \frac{1}{24} \quad (13)$$

Where d_p is the bubble size presented as diameter, C_D is the drag force coefficient and Re is the relative Reynolds number. [26]

$$Re = \frac{\rho d_p |u - u_p|}{\mu} \quad (14)$$

$$C_D = \frac{2}{3} E_0^{0.5} \quad (15)$$

$$E_0 = \frac{g(\rho - \rho_p) d_p^2}{\sigma} \quad (16)$$

The additional virtual mass force, which can be expressed as following:

$$\vec{F}_{VM} = -C_{VM} \frac{\rho}{\rho_p} \left(\vec{u}_p \nabla \vec{u} - \frac{d\vec{u}_p}{dt} \right) \quad (17)$$

Where C_{VM} value is 0.5, which is the virtual mass factor. The argon gas density is determined by using the ideal gas law based on bubble local according to the static pressure at certain position and a given constant temperature of 1875K. This density is employed to simulate the diameter change as bubbles rising with the pressure gradient change inside the ladle. The maximum bubble diameter in a ladle is reported by Aoki et al. [27]

$$d_{bubble-max} = 0.35 \left(Q^2 / g \right)^{0.2} \quad (18)$$

Where Q is the injected argon gas flow rate by volume. Fukuji et al. [28] made a serial of assumptions about bubble size, one of them is that the average bubble size is 50% of the maximum bubble size.

A bubble coalescence and break-up model is used to calculate the variation of bubble size. Laux et al. [29] created the basic fundamental theory and Cloete et al.[30] and Pan [31] developed improvement modification. In a turbulent flow field, the equilibrium bubble diameter is expressed as following:

$$d_b^{eq} = C_1 * \alpha_b^{0.5} \frac{(\sigma/\rho)^{0.6}}{\varepsilon^{0.4}} (\mu_b/\mu)^{0.25} + C_2 \quad (19)$$

where ε is the turbulent kinetic energy dissipation, μ_b is the bubble phase viscosity, σ is the surface tension between argon bubble and the other continuity fluid, and α_b is the bubble concentration. C_1 is a constant which is dimensionless, and C_2 present the minimum bubble size. [32] The relax time needed for bubbles get the equilibrium diameter based on bubble location as given by equation (20). The relax time get command of the bubble coalescence and break-up process speed. The relaxation is derived by the microscale in turbulence flow and presents the smallest timescale in the multiphase flow. The relax time τ_{rel} is given:

$$\tau_{rel} = \begin{cases} \tau_B \\ \tau_C \end{cases} \quad (20)$$

$$\tau_{rel} = |\tau_{rel}, \tau_k|_{max} \quad (21)$$

Here τ_k is the microscale in turbulence flow, which is represented by equation (22):

$$\tau_k = 6 \sqrt{\frac{\bar{v}}{\varepsilon}} \quad (22)$$

where v is the kinetic viscosity inside the fluid. The time scale of break-up τ_B and time scale of coalescence τ_C are predicted by equations (23) and (24):

$$\tau_B = d_b^{\frac{2}{3}} \varepsilon^{-\frac{1}{3}} \quad (23)$$

$$\tau_C = \frac{d_b}{0.2 \cdot 6 \cdot \sqrt{\alpha_b k}} \quad (24)$$

The assumption [33] has been made, that if the argon bubble size is less than the equilibrium bubble diameter, the coalescence happens between two small bubbles; and if the bubble diameter is larger than the equilibrium bubble diameter, the break-up process happens more frequently.

Based on these theories, several user-defined functions are developed to simulate the drag force, the density change of argon gas due to the decrease of absolute pressure, and the coalescence and breakup of argon bubbles. Moreover, the argon bubbles will be deleted when the volume fraction of argon gas is larger than 0.95 at the moment when the bubbles reach the free surface of slag layer and are about to enter the atmosphere.

2.3.2 CFD model for inclusion behavior

2.3.2.1 Population balance model

For the Population balance model description, inclusion number density $n(V_i)$ has been posted, and the equation of the transportation for the number density $n(V_i)$ expressed as follows:

$$\frac{\partial n(V_i)}{\partial t} + \nabla \cdot (\vec{\mu}_p n(V_i)) = \frac{1}{2} \int_0^{V_i} \beta(V_i - V_j) n(V_i - V) n V_j dV_j - \int_0^{V_{\max}} \beta(V_i, V_j) n(V_i) dV_j + S_i \quad (25)$$

where $\beta(V_i, V_j)$ describes the inclusion collision rate and V_i is the inclusion volume fraction of group i . Terms at the right side of the equation are the growth rates and death rates because of the collision and nucleation of smaller inclusion, and the inclusion removal rates.

The population balance equation can be determined by the continuum method. The different size of the inclusion can be divided into a certain set of groups. Because the number of inclusion is too large to calculate one by one like bubble in DPM. The advantage of this approach is the the PSD has been given directly. So that, the Eq. (26) can be expressed as a term of the volume fraction for each particle's size i . Furthermore, to ensure the mass conservation of inclusion, the Eq. (3) should be satisfied:

$$\alpha_i = \sum_{i=0}^{N-1} \alpha_i \quad (26)$$

$$S_i = \sum_{i=0}^{N-1} \rho V_i S_i \quad (27)$$

Where S_i and α_i are the source term and volume fraction of inclusion phase.

$$S_i = S_i^{\text{wall}} + S_i^{\text{F}} + S_i^{\text{BF}} + S_i^{\text{TR}} + S_i^{\text{TS}} + S_i^{\text{wake}} \quad (28)$$

$S_i^{\text{wall}}, S_i^{\text{F}}, S_i^{\text{BF}}, S_i^{\text{TR}}, S_i^{\text{TS}}, S_i^{\text{wake}}$ present the mass source terms of inclusion removal due to main three theory, including removal through wall, slag and bubble.

In a gas-stirred turbulent flow system, six inclusion removal mechanisms including refractory adhesion, inclusion removal via their own buoyancy floatation to the slag layer, inclusion-bubble

buoyancy collision, inclusion-bubble random collision, inclusion-bubble shear collision, and bubble wake capture theory are investigated in this study.

I. Inclusions removal due to refractory adhesion

In a gas-stirred ladle, when the inclusions diffuse to the refractory lining, the inclusion will be attached on the wall, and the transport of inclusion to the wall surface is considered as a diffusion and transport process, which is determined by the near wall liquid steel turbulent condition.

$$S_i^W = \frac{0.0062\varepsilon^{\frac{3}{4}}}{v^{\frac{5}{4}}} \frac{A_s}{V_{cell}} r_i^2 n(V_i, t) \quad (29)$$

II. Inclusion removal via their own buoyancy

For single inclusion, which is in the flow field, could be captured by the slag layer at the top of the ladle due to their own floating motion including turbulent fluctuating floatation and Stokes floatation. In this mechanism, the rate of inclusion removal because of inclusion floatation can be shown as follows:

$$S_i^S = \frac{dn}{dt} = \frac{n_i \cdot u_{st}}{h} \quad (30)$$

III. Inclusions removal via inclusion-bubble buoyancy collision

Inside the gas-stirring multiphase flow model, the bubble–inclusion buoyancy collision because the difference rising velocity between argon bubble and small inclusion. This mechanism is similar to the inclusion-inclusion coalescence, the inclusion–bubble collision efficiency can be calculated by using Dukhin’s model. So that, the removal rate due to bubble floatation can be expressed by using following equation:

$$S_i^{TR} = C \frac{\pi}{4} (d_i^2 + d_g^2) E_s^{g-p} \frac{6\alpha_g}{\pi d_g^3} n(V_i, t) \quad (31)$$

IV. Inclusions removal via inclusion-bubble random collision

For this gas-stirring system under the turbulent flow condition, inclusion can be dragged by velocity patterns in the gas-stirring system, once the inclusion size is larger than the Kolmogorov microscale, which calculated based on the flow field, in the argon bubble plume region. The main reason of bubble-inclusion collision is fluid particles like inclusion has the turbulent random motion, the theory is similar to the inclusion-inclusion turbulent collision, and the total inclusion removal rate via inclusion-bubble random collision can be expressed by using following equations:

For $d_i > \eta$,

$$S_i^{TR} = C \frac{\pi}{4} (d_i + d_g)^2 (\varepsilon d_i)^{\frac{1}{3}} \frac{6\alpha_g}{\pi d_g^3} n(V_i, t) \quad (32)$$

For $d_i < \eta$,

$$S_i^{TR} = C \frac{\pi}{4} (d_i + d_g)^2 (\varepsilon \eta)^{\frac{1}{3}} \left(\frac{d_i}{\eta}\right)^3 \frac{6\alpha_g}{\pi d_g^3} n(V_i, t) \quad (33)$$

V. Inclusions removal via inclusion-bubble turbulent shear collision

The inclusion removal through turbulence shear collision theory is similar to the inclusion–inclusion coalescence in turbulent eddy, which happened in small size particles inside the gas-stirring system. The bubble-inclusion collision process can be described through analogous mechanism for small size bubble. In the gas-stirred ladle, once the eddy larger than bubble size, it will have enough energy for capturing and carrying both bubble and inclusion. The local shear rate, which has an efficiency describe capture, decides the bubble-inclusion shear collision rate in the turbulence flow, and the inclusion removal rate through bubble-inclusion turbulent shear collision can be shown as following equation:

$$S_i^{TS} = 1.294 \zeta_{eff}^{p-g} \left(\frac{\varepsilon}{\nu}\right)^{0.5} (r_i + r_g)^3 \frac{6\alpha_g}{\pi d_g^3} n(V_i, t) \quad (34)$$

where ζ_{eff}^{p-g} the efficiency rate for turbulent shear collision capture of both bubble and inclusion.

VI. Inclusions removal via bubble wake capture

In gas-stirring system, because of the rising of the bubble, the wake of the bubble is generated at the same time. Since the size different between the bubble and inclusion is large. The inclusion which near the slag and steel interface boundary can be captured into this wake, then the inclusion will be carried to the slag layer. The removal rate for inclusion due to the argon bubble wake capture can be expressed as following equation:

$$S_i^{Wake} = 3.45 \alpha_g (u_g + u_l) \frac{A_s}{V_{cell}} n(V_i, t) \quad (35)$$

2.4 Multiphase Flow Validation

In order to validate the fluid flow dynamic model. The simulation result is compared against plant measurement data in real work condition. Because only one flow rate has been applied at current operation condition, 30scfm (80L/min) argon flow rate results has been compared.

2.4.1 Comparison Results

Validation for slag eye size between CFD results with industry plant measurement data had been done. The Table 2.1 shows the validation conditions.

Table 2.1 Initial conditions for full-scale ladle

Name	Condition
Argon volume flow rate per inlet	850 L/min
Pressure outlet	101325 Pa (1 atm)
Boundary wall	no-slip
Initial bubble diameter	0.014 m
Slag thickness	0.28 m
Liquid steel depth	2.67 m

The slag eye size (mean value of two slag diameter) from CFD simulation is 0.80 m, and slag eye size (mean value of two slag diameter) from Nucor Steel is 0.73 m. The VOF method and Eulerian method results have been compared. For Eulerian approach, the error between CFD and measurements results is 8.75%. Table 2.2 shows the detailed comparison data.

Table 2.2 Flow model validation

	Slag eye size (m)	Error (%)
Eulerian-Eulerian model	0.80 (31.5 in)	8.75
Eulerian-VOF model	0.79 (31.2 in)	7.50
Nucor plant measurements	0.7-0.79 (28-31 in) out of 5 measurement	—

CHAPTER 3. GAS-STIRRED LADLE INCLUSION REMOVAL SIMULATION

3.1 Computational Domain

For the full scale three-dimension multiphase flow simulation model of the gas-stirred ladle has been developed. The parameters of this furnace have been shown

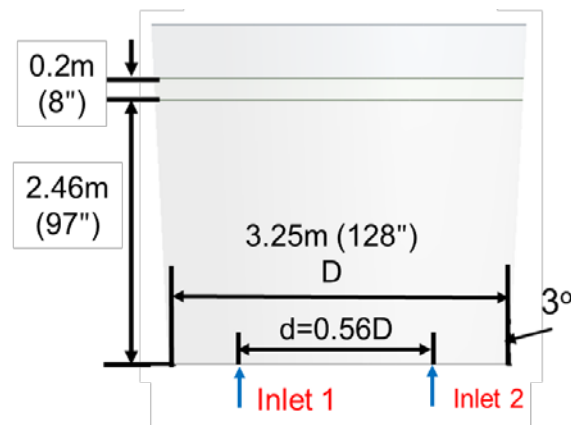
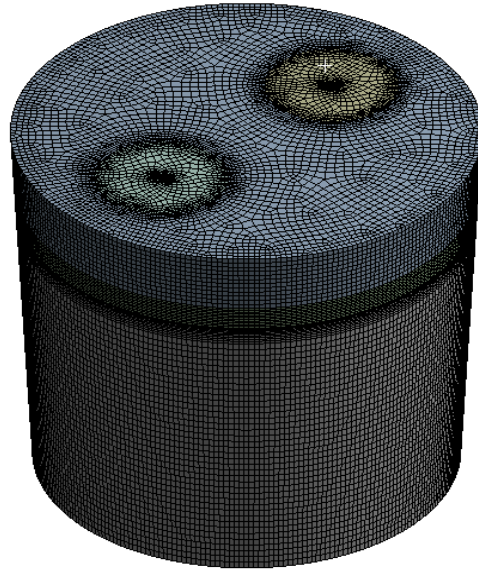
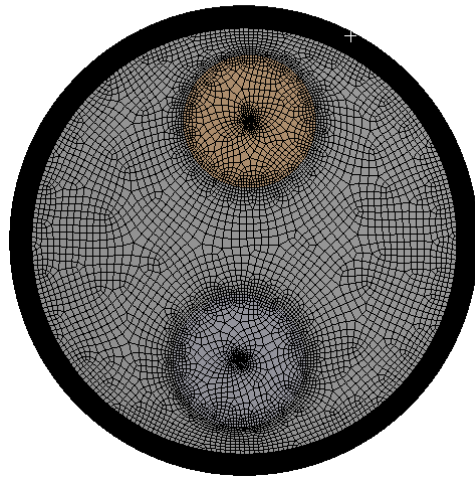


Figure 3.1 Computational domain of Nucor Decatur gas-stirred ladle

In order to store the physical properties for the numerical simulation, the computational domain has been partitioned by small mesh. Figure 3.2 shows the furnace mesh. Based on the mesh sensitivity study and expresses the appropriate elements number is 1.1 million. The average mesh quality is 0.8967, which is near one, the mesh quality is acceptable.



a)



b)

Figure 3.2 Calculation Mesh: a) front view b) bottom view

3.2 Boundary Conditions

Argon inlet condition: For inclusion removal process, gentle stirring is needed. The argon gas injected from bottom plugs is 5scfm/plug. Figure 3.3 shows the slag shape after the multiphase flow reached “quasi steady state”.

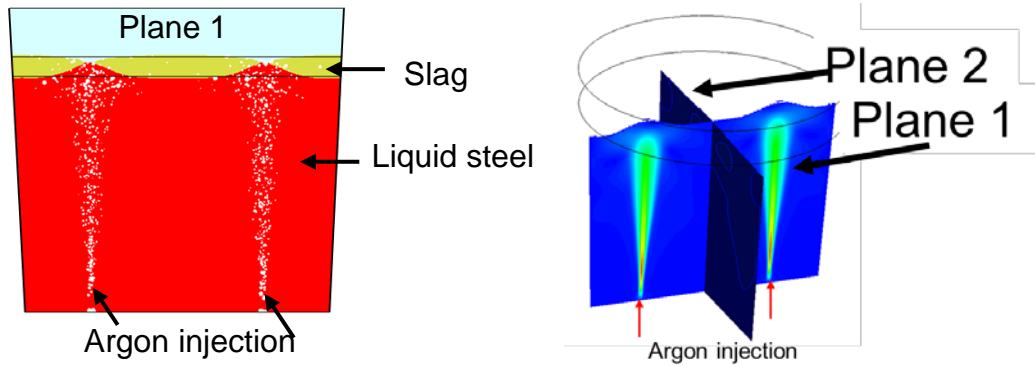


Figure 3.3 Multiphase flow a) The volume fraction of three phases
b) The velocity of steel

Outlet conditions: The top outlet is set as the pressure outlet, and the calculation of the inclusion removal phenomena is under isothermal condition, so there is no need to specify the pressure difference between the ladle inside and outside.

Wall condition: Wall surfaces are treated as non-slip walls, the standard wall function has been employed at the near-wall area.

Inclusion initial distribution: The inclusion number density at $t=0s$ is $4.23E+12/m^3$ [21]. The constant inclusion size distribution is assumed as five micro meter ($5\mu m$).

3.3 Results and Analysis of Baseline Case Simulation

The liquid steel initial condition is static, the argon gas is blowing from the bottom plugs of the steel to propel the steel move gently. Then, the flow properties inclusion turbulence kinetic energy, velocity almost keep fluctuating within a similar range, this phenomena is "quasi steady- state" process. The "quasi steady-state" process standard a certain flow condition, which means in a long time scale of this multiphase flow, the gas concentration and the average flow velocity changes small almost no change with time or stabilize around in a certain range. Based on the previous results, the quasi-steady state can be reached at 80s since bubble blowing from bottom. [32] According to that, the further study can be developed based on the quasi steady-state flow condition.

3.3.1 Multiphase Flow development

The bubble behavior in a full scale steel ladle has been simulated after the model validation. The first 30 seconds of the flow field is shown in Figure 3.4, in which the yellow layer represents the slag layer. The injected argon gas velocity vector at different times, as well as slag shape, shown in these series of figures. It takes approximately 2.0 s for bubbles to reach the free surface, there is no slag eye opened under this gentle argon injection rate. The bubble plume looks like a mushroom as a result of the accumulation effect of the top part of the plume when pushing the slag away. After 30s, the shape of the “mushroom” no longer changes. Those flow field characters, including three phases’ pressure, velocity, volume fraction and turbulence characters can be imported to the inclusion removal simulation.

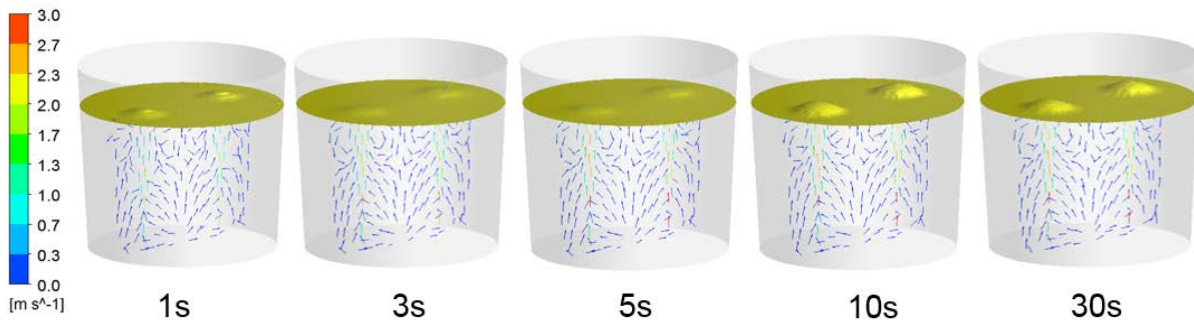


Figure 3.4 Slag movement within the first 30s inside the ladle for Baseline Case ($Q = 5\text{scfm}$).

Since the inclusion removal process is highly related to slag eye size and location, the effect of argon flow rate to slag eye size has been analyzed. The diameter change of slag eyes with changing argon flow rate is shown in Figure 3.5. The diameter of the slag eye is expanded when the argon gas flow rate increases. In the baseline case, the argon flow rate is 5 SCFM/plug, which is too small to push the slag out then create a slag eye, when the argon flow rate is 30scfm (850 L/min) per plug which is the normal mixing treatment condition, the diameter of the slag eye is 0.79 m.

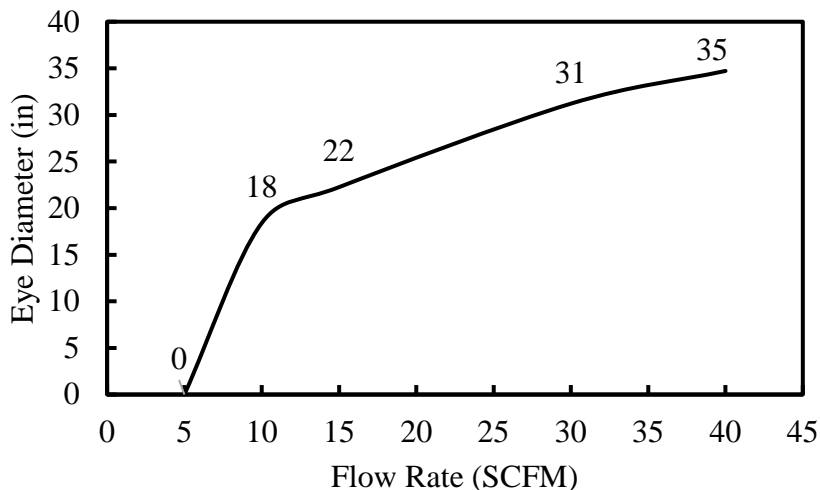


Figure 3.5 Effect of argon gas flow rate on slag eye size

3.3.2 Gas bubble distribution analysis

A detailed plot of bubble plumes at 10 s is shown in Figure 3.7. Larger bubbles are formed at the outer boundary of the bubble plume as a result of less turbulence mixing, which promotes coalescence. The bubbles in the center region of the plume are easy to break-up, resulting in smaller bubbles. The initial bubble diameter is 0.55in (0.014m), the weight percentage of bubbles smaller than the initial diameter is 76.8% while the weight percentage of bubbles larger than the initial diameter is 23.2%. This means that in the baseline case, breakup is more dominant than coalescence.

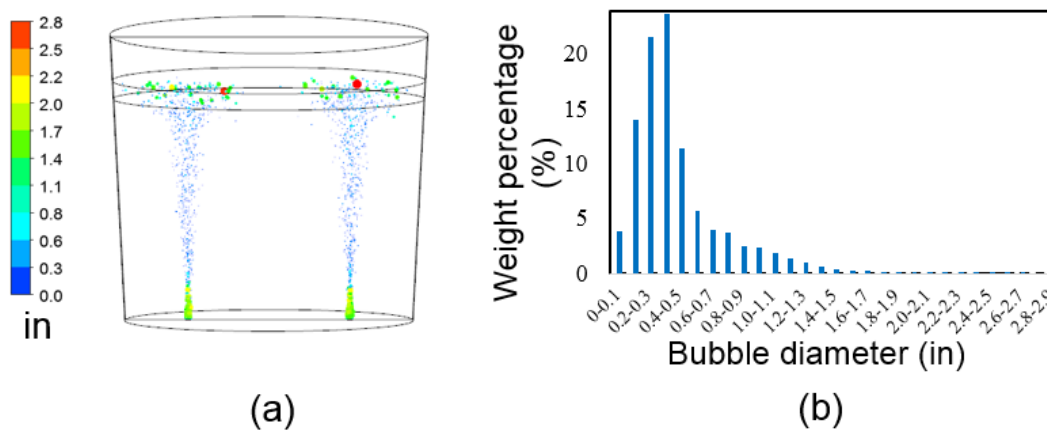


Figure 3.6 Gas bubble development: (a) contour of gas bubble diameter.
(b) Bubble weight percentage

Since the inclusion removal efficiency is sensitive to argon bubble diameter, the effect of the bubble initial diameter on the bubble ultimate distribution and slag eye size has been investigated. As shown in Figure 3.8, no matter what value is chosen for the bubble initial diameter, the overall bubble weight distribution is very close for these three cases. That's because the bubble size distribution is effected more by the flow field inside the ladle. Most of the bubbles have a diameter between 0.1in to 0.6in. It appears that the bubble size reaches an “equilibrium” size distribution independent of the initial bubble diameter.

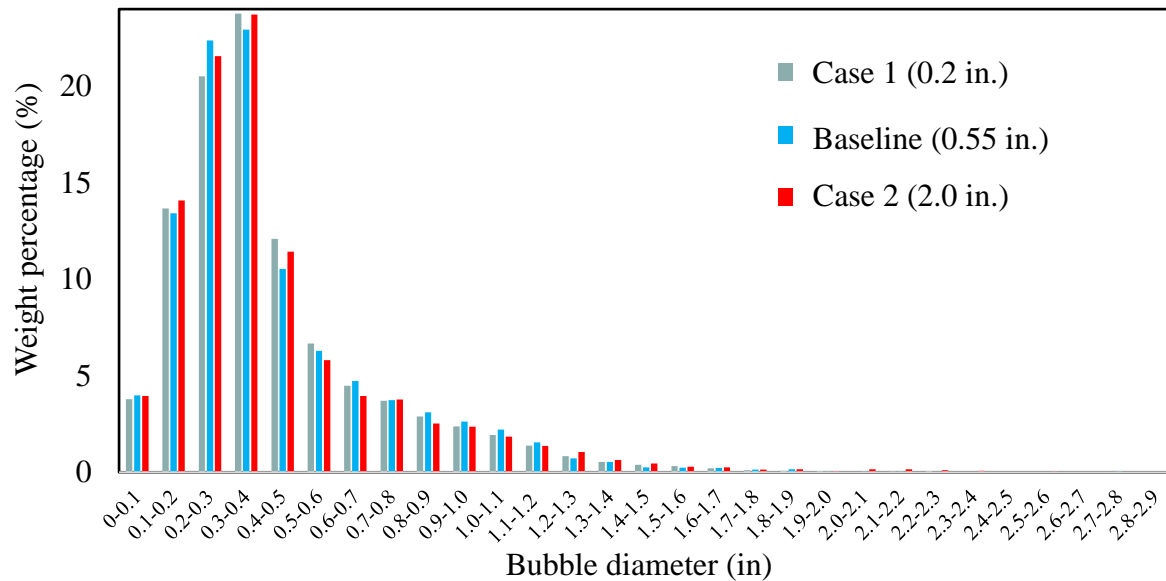


Figure 3.7 Bubble diameter distribution based on weight percentage of total weight of bubbles.

3.3.3 Flow characteristics

The streamline at the center planes has been shown in Figure 3.8. The typical flow patterns distribution in the baseline case for ladle with two plugs were placed diametrical and were opposed as ratio 0.6 of bottom radius. The upstream jets due to gas injections from the two plugs form two bubble plumes and develop along with their rise; the two plumes divide into two streams and flow going down along the refractory. Figure 3.8 also presents two different symmetry flow circulations. The first recirculation plane is crossing two plugs, another plane is perpendicular to the first recirculation plane, and the plane between two plugs only shows one direction circulation.

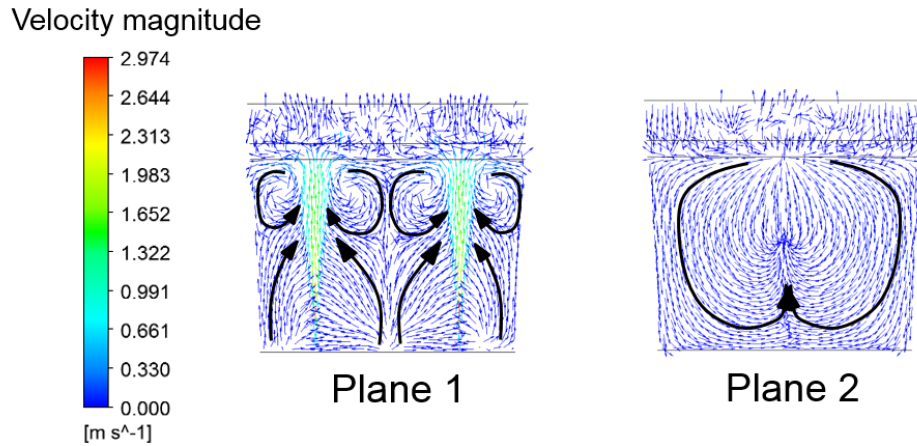


Figure 3.8 Flow behavior: Streamline at the center planes

3.3.4 Inclusion removal analysis

Figure 3.9 shows the concentration of inclusion in Nucor Steel Decatur ladle with eccentric tuyeres. Figure 3.10 shows the overall inclusion number of the density change with gas blowing time. Figure 3.9 shows inclusion concentration distribution with a radius of $5\mu\text{m}$, the initial number density is $4.23\text{E}+10^{12}/\text{m}^3$. It could be witnessed that the inclusion concentration decreases regularly and steadily in the whole ladle as the development of the gas-stirred process. Inclusion concentration gradient turn to small, becoming to the more uniform distribution in the steel along with the gentle argon gas blowing from bottom. The content of inclusion is highest at the corner where the ladle refractory meet with the ladle bottom wall. That is because the flow has stronger turbulence kinetic energy at the bubble region but get lower turbulence kinetic energy at the bottom and the wall nearing areas, which can be proven by the velocity distribution inside the ladle (Figure 3.8).

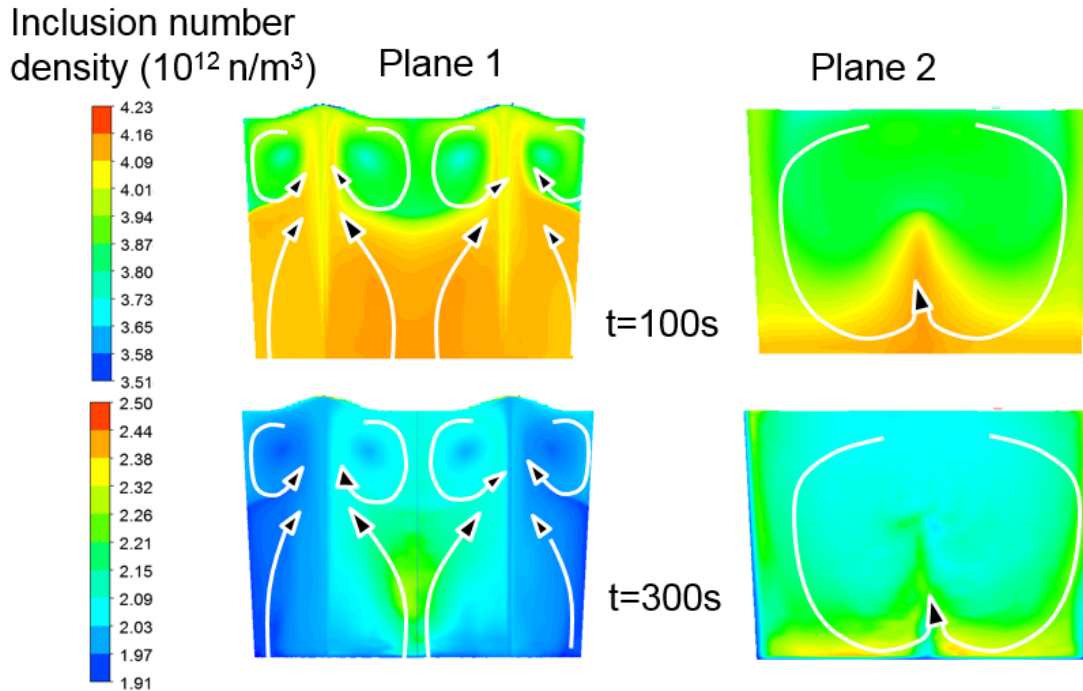


Figure 3.9 Inclusion concentration distribution with a radius of $5\mu\text{m}$ at 100s, 300s.

The trend of overall inclusion number density with time is shown at Figure 3.10. At the beginning, several seconds of the removal process, the removal rate is slow, the reason for this phenomenon is that in the first seconds, the bubble did not fully generate. Since the bubble-inclusion collision is the main mechanisms for inclusion removal from ladle, the bubble-inclusion collision rate is slow as well. Once the argon bubble plume fully developed, the speed of inclusion removal turn to fast until the inclusion number density decreases to half the amount. The removal rate drops because the inclusion concentration is decreased a lot even if the bubble plume is already fully developed.

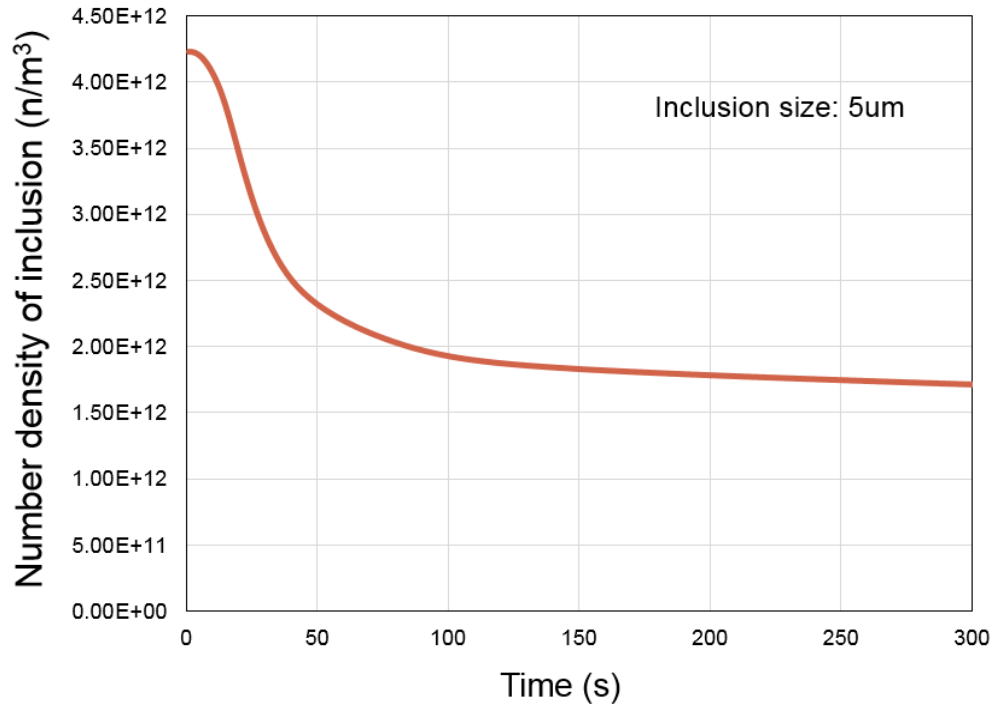


Figure 3.10 Overall inclusion number density change with gas blowing time

The final inclusion removal ratio is calculated based on following equation:

$$\text{Removal ratio} = \frac{n(V_i, 0) - n(V_i, t = 300s)}{n(V_i, 0)} * 100\% \quad (36)$$

For 5 μ m inclusion, the 300s removal ratio is 59.6%. Figure 3.11 shows the contribution of different removal mechanisms for the inclusion contents. The results expressed in this figure was obtained by analyzing the respective removal theory without considering any phenomena of growth or aggregation. The bubble-inclusion collision, including turbulence buoyancy collision, turbulence random collision, turbulence shear collision and bubble wake capture collision is the prevailing mechanism of inclusion removal, takes 99% in this baseline case; the slag capture also contributes to remove a quite amount of inclusion, even though the removal ratio of inclusion through the wall adhesion is relatively low.

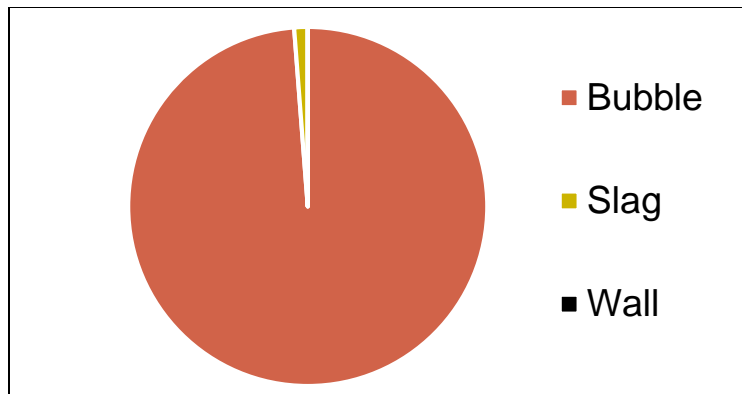


Figure 3.11 Effect of different mechanism on inclusion removal efficiency

From figure 3.12, it is obvious that the inclusion removal efficiency of wall adhesion is low, only take less than one percent of the total removal ratio. The removal efficiency of flotation for inclusion with $5\mu\text{m}$ is low as well, while that of inclusions with larger diameter is relatively significant, since the large inclusion have higher flotation velocity than do small inclusion. It is smaller possibility that small size inclusion can be removed through stokes flotation; inclusion can be removed by carrying to the slag layer transport with the bubble after colliding with it.

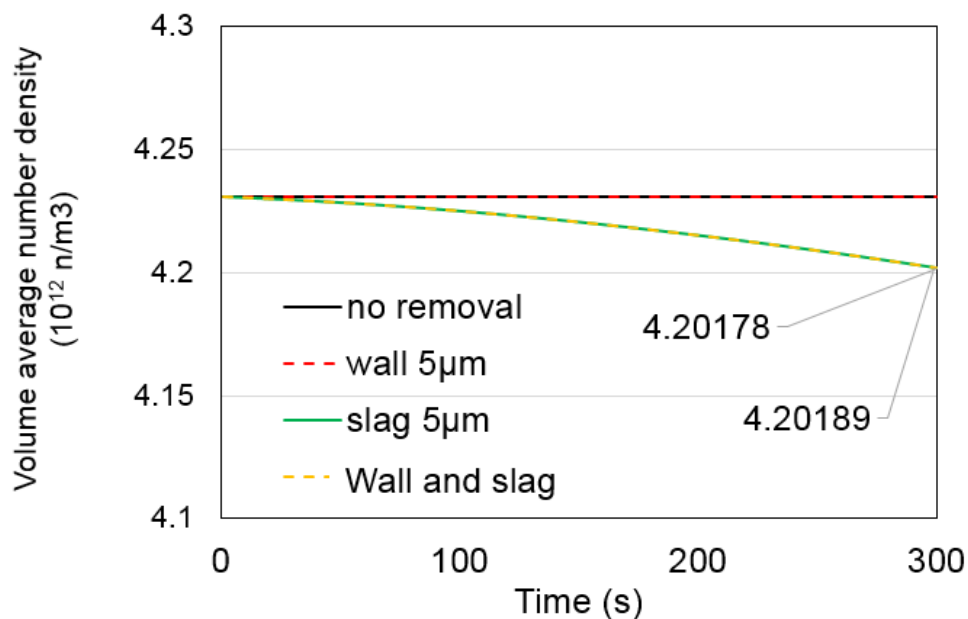


Figure 3.12 Inclusion removal to the wall and slag

3.4 Parametric Study

Without considering the theory of inclusion growth, six types of mechanisms for inclusion removal, such as wall adhesion, inclusion captured by slag layer, inclusion-bubble buoyancy collision, inclusion-bubble turbulence random collision, inclusion-bubble turbulence shear collision and bubble wake capture. The parametric studies related to inclusion size and removal mechanisms have been conducted.

3.4.1 Inclusion size

Figure 3.13 shows in the 5 SCFM gentle gas flow condition, the inclusion number densities change of different size with times. For a certain size of inclusion, the number density change only related to the inclusion removal is based on previous assumptions. Since the bubble-inclusion collision is the main mechanism of inclusion removal, and the collision rate is a function of inclusion size. The large inclusion will lead to a higher removal rate.

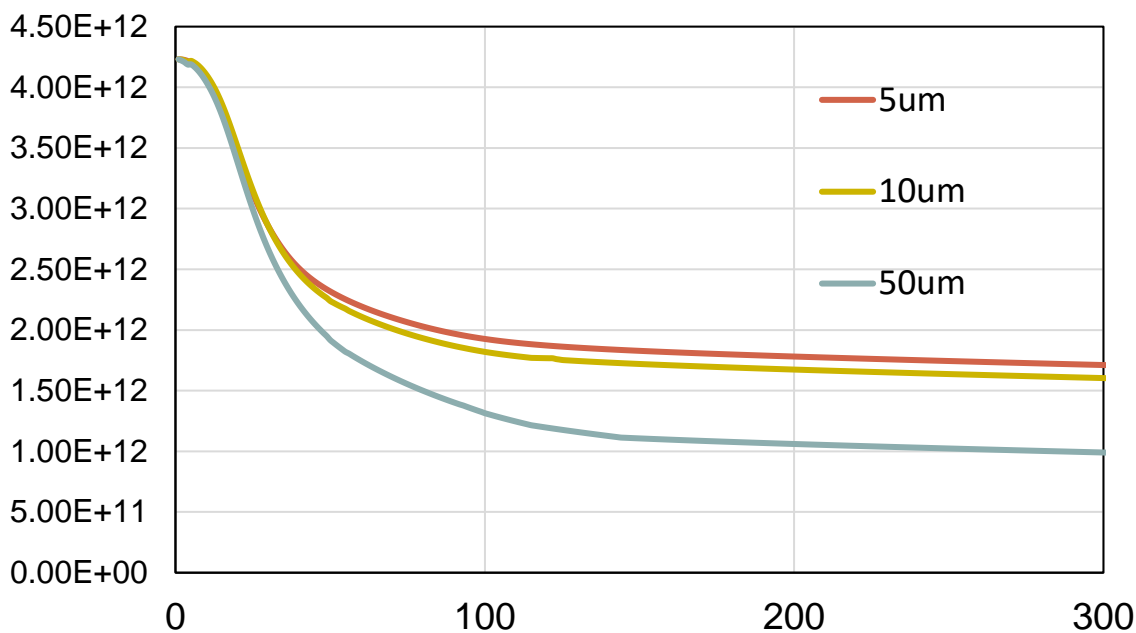


Figure 3.13 The inclusion number density change of different inclusion size with times

Table 3.1 Inclusion removal ratio of different inclusion size

Inclusion size (μm)	5	10	50
Removal rate	59.6%	62.2%	76.6%

3.4.2 Results comparison

Results comparison between this study and Lou et al.'s CFD work has been conducted. In this study, the inclusion formation and aggregation have been neglected, the size of inclusion keep constant. Lou et al. employed the inclusion growth model, divided inclusion into 18 groups, size from $4\mu m$ to $100\mu m$, but keeping the bubble at a constant value. Lou et al. ignored the slag and air phase inside the ladle and only focused on the steel and inclusion phase. The single plug ladle has been introduced under gentle stirring condition.

Table 3.2 Comparison between Lou et al.'s CFD with current work

Parameters	Lou et al. (2013)	Inclusion $5\mu m$	Inclusion $50\mu m$
Melt depth (m)	3.115	2.46	2.46
Slag depth (m)	-	0.2	0.2
Plug distance ratio ($\frac{\text{Distance from center to plug}}{\text{Floor radius}}$)	Single plug	0.56	0.56
Bubble diameter	15mm	5~17mm	5~17mm
Final inclusion size	4~100 μm	5 μm	50 μm
Argon flow rate (m^3/s)	0.000059 (3.531 CFM)	0.00472 (10 SCFM)	0.00472 (10 SCFM)
Removal ratio for 5 μm inclusion	$\approx 78.6\%$	59.9%	76.6%

3.4.3 Analysis of different removal mechanisms

Figure 3.14 presents the inclusion removal efficiency due to various mechanisms for three different inclusion sizes. With the increase in the inclusion size, the inclusion removal ratio by slag capture is noticeably increased because large inclusions have higher flotation velocities than small ones; the larger inclusion have a much higher probability of collision with a gas bubble which supports higher attachment probability; the wall adhesion ratio is still low even if the inclusion is larger than before. The total removal efficiency increases.

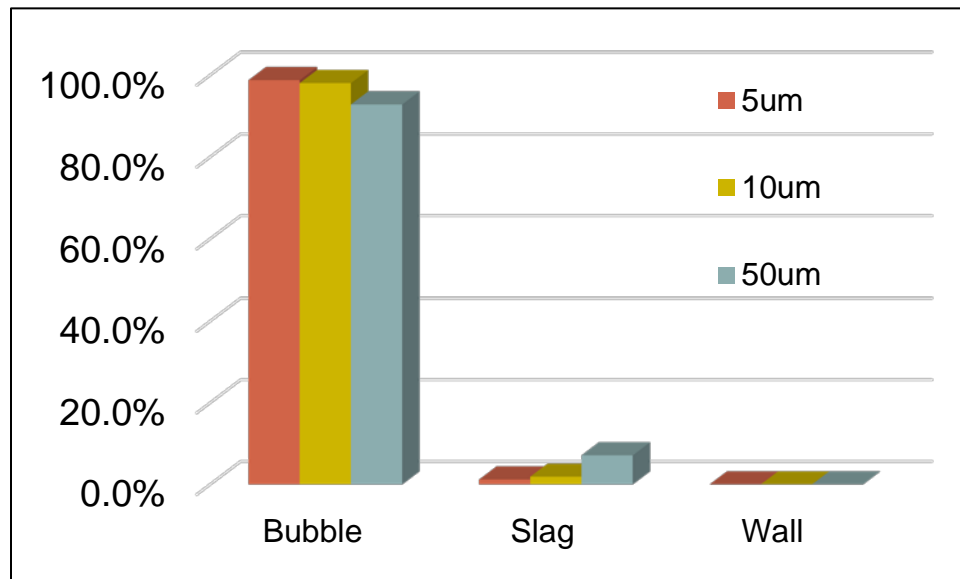


Figure 3.14 The inclusion removal efficiency due to various mechanisms for $5\mu\text{m}$, $10\mu\text{m}$ $50\mu\text{m}$ inclusion size

CHAPTER 4. CONCLUSIONS

4.1 Conclusions

A three dimensional turbulence multiphase (three phase: steel, slag and air) flow model has been developed. The Eulerian-Eulerian approach was applied to predict flow, comprehensive argon bubble coalescence and break-up model was developed as well. The models were further validated with industry measurements. The coupled CFD-PBM model has been introduced to describe the inclusion removal process. Multiple sources of inclusion removal have been studied and used into simulation work by writing them into User defined code.

The baseline case of the gas-stirred flow has been validated. The gas-stirring flow reaches quasi-steady state after the gas blowing certain time. In the argon bubble plume areas existing stronger turbulence effects.

A comprehensive inclusion removal model has been developed with reasonable assumptions, which are ready to predict removal rate and ratio for different ladle designs. Through the analysis of baseline case, the main mechanism of inclusion removal, which is inclusion-bubble collision, has been found. The parametric study on the inclusion size was conducted. The results show that as the inclusion size increases, the removal ratio increases as well. Under 50um condition, compared to baseline case, the inclusion removal ratio increases by 27%. With the increase of inclusion diameter, the removal by slag makes more of a contribution to the removal process, because large inclusion has a higher stoke velocity.

LIST OF REFERENCES

- [1] Zhang, L., & Thomas, B. G. (2003). XXIV National Steelmaking Symposium. Morelia, Mich, Mexico, 138.
- [2] O'Malley, R. J. (2017, May). Inclusion evolution and removal in ladle refining. In AISTech 2017 conference and exposition, Nashville, TN (pp. 8-11).
- [3] You, D., Michelic, S. K., Presoly, P., Liu, J., & Bernhard, C. (2017). Modeling inclusion formation during solidification of steel: A review. *Metals*, 7(11), 460.
- [4] Nakanishi, K., & Szekely, J. (1975). Deoxidation kinetics in a turbulent flow field. *Trans. Iron Steel Inst. Jpn.*, 15(10), 522-530.
- [5] Roy, T. D., Majumdar, A. K., & Spalding, D. B. (1978). Numerical prediction of recirculation flows with free convection encountered in gas-agitated reactors. *Applied Mathematical Modelling*, 2(3), 146-150.
- [6] Johansen, S. T., Robertson, D. G. C., Woje, K., & Engh, T. A. (1988). Fluid dynamics in bubble stirred ladles: Part I. Experiments. *Metallurgical Transactions B*, 19(5), 745-754.
- [7] Mazumdar, D., & Guthrie, R. I. (2010). Modeling energy dissipation in slag-covered steel baths in steelmaking ladles. *Metallurgical and Materials Transactions B*, 41(5), 976-989.
- [8] Zhang, L. (2000). Mathematical simulation of fluid flow in gas-stirred liquid systems. *Modelling and Simulation in Materials Science and Engineering*, 8(4), 463.
- [9] Cloete, S. W. P. (2008). A mathematical modelling study of fluid flow and mixing in gas stirred ladles (Doctoral dissertation, Stellenbosch: Stellenbosch University).
- [10] Cao, Q., & Nastac, L. (2018). Mathematical Investigation of Fluid Flow, Mass Transfer, and Slag-steel Interfacial Behavior in Gas-stirred Ladles. *Metallurgical and Materials Transactions B*, 49(3), 1388-1404.
- [11] Guo, D., & Irons, G. A. (2000). Modeling of gas-liquid reactions in ladle metallurgy: Part II. Numerical simulation. *Metallurgical and Materials Transactions B*, 31(6), 1457-1464.
- [12] Zhu, M., Zheng, S., Huang, Z., & Gu, W. (2005). Numerical Simulation of Nonmetallic Inclusions Behaviour in Gas-Stirred Ladles. *Steel research international*, 76(10), 718-722.
- [13] Nakanishi K. & Szekely J.(1975) Deoxidation Kinetics In A Turbulent Flow Field, *Trans. Iron Steel Inst. Jpn.*, vol(15) 522-530.

- [14] Shirabe, K., & Szekely, J. (1983). A mathematical model of fluid flow and inclusion coalescence in the RH vacuum degassing system. *Transactions of the Iron and Steel Institute of Japan*, 23(6), 465-474.
- [15] Johansen, T., Boysan, F. & Engh, T.A., (1986), "Numerical Calculation of Removal of Inclusions and Dissolution of Refractory in a Bubble Stirred Ladle", *The 4th Japan-Nordic Countries Joint Symp on Science and Technology of Process Metallurgy*, Iron Steel Inst. Jpn., 182-215.
- [16] Hodgson, P. D. (1996). Microstructure modelling for property prediction and control. *Journal of Materials Processing Technology*, 60(1-4), 27-33.
- [17] Fuchigami, K., WAKOH, M., Imamura, N., ENDOH, K., Kiyose, A., & Sawada, I. (1999). Analysis of inclusion behavior in a ladle refining process by a newly developed coagulation model. *Tetsu-to-Hagané*, 85(5), 368-374.
- [18] Miki, Y., & Thomas, B. G. (1999). Modeling of inclusion removal in a tundish. *Metallurgical and Materials Transactions B*, 30(4), 639-654.
- [19] Sheng, D. Y., Söder, M., Jönsson, P., & Jonsson, L. (2002). Modeling micro-inclusion growth and separation in gas-stirred ladles. *Scandinavian journal of metallurgy*, 31(2), 134-147.
- [20] Söder, M., Jönsson, P., & Jonsson, L. (2004). Inclusion Growth and Removal in Gas-Stirred Ladles. *Steel research international*, 75(2), 128-138.
- [21] Lou, W., & Zhu, M. (2015). Numerical Simulation of Desulfurization Behavior in Gas-Stirred Ladles. In *TMS 2015 144th Annual Meeting & Exhibition* (pp. 771-781). Springer, Cham.
- [22] Wang, L. T., Peng, S. H., Zhang, Q. Y., & Li, Z. B. (2006). Mathematical Model for Growth and Removal of Inclusions in Molten Steel under Gas-stirring Conditions. *steel research international*, 77(1), 25-31.
- [23] SMSVC (2017) Computational Studies and Optimization of Inclusion removal In a Steel Ladle progress report.
- [24] Yan, H. J., Liu, F. K., Zhang, Z. Y., Gao, Q., Liu, L., Cui, Z. X., & Shen, D. B. (2012). Influence of lance arrangement on bottom-blowing bath smelting process. *Chin. J. Nonferrous Met*, 22, 2393-2400.
- [25] ANSYS Theory Guide, Discrete Phase, (2017).

- [26] Xia, J. L., Ahokainen, T., & Holappa, L. (2001). Analysis of flows in a ladle with gas-stirred melt. *Scandinavian journal of metallurgy*, 30(2), 69-76.
- [27] Aoki, J., Thomas, B. G., Peter, J., & Peaslee, K. D. (2004). Experimental and theoretical investigation of mixing in a bottom gas-stirred ladle.
- [28] Yamashita, F., Mori, Y., & Fujita, S. (1979). Sizes and size distributions of bubbles in a bubble column. *Journal of Chemical Engineering of Japan*, 12(1), 5-9.
- [29] Laux, H., & Johansen, S. T. (1999). A CFD analysis of the air entrainment rate due to a plunging steel jet combining mathematical models for dispersed and separated multiphase flows. *Fluid Flow Phenomena in Metal Processing*.
- [30] Cloete, S., Olsen, J. E., & Skjetne, P. (2009). CFD modeling of plume and free surface behavior resulting from a sub-sea gas release. *Applied Ocean Research*, 31(3), 220-225.
- [31] Pan, Q. (2014). Modelling of turbulent flows with strong dispersed phase-continuous fluid interactions.
- [32] Liu, H., Qi, Z., & Xu, M. (2011). Numerical Simulation of Fluid Flow and Interfacial Behavior in Three-phase Argon-Stirred Ladles with One Plug and Dual Plugs. *Steel research international*, 82(4), 440-458.
- [33] Peranandhanthan, M., & Mazumdar, D. (2010). Modeling of slag eye area in argon stirred ladles. *ISIJ international*, 50(11), 1622-1631.

PUBLICATIONS

Tang G, Liu W, Silaen A K, et al. Modeling of Post-Combustion in an Electric Arc Furnace[C] // ASME 2017 International Mechanical Engineering Congress and Exposition. 2017:V008T10A034.

Liu W, Lee J, et al. Argon Bubble Coalescence and Breakup in a Steel Ladle with Bottom Plugs [J] Journal of steel research international (accepted).